

## Article

# Electric Field-Driven Air Purification Filter for High Efficiency Removal of PM<sub>2.5</sub> and SO<sub>2</sub>: Local Electric Field Induction and External Electric Field Enhancement

Jian Li <sup>1,2</sup>, Qingyun Sun <sup>2</sup>, Zhongxin Ping <sup>2</sup>, Yihong Gao <sup>2</sup>, Peiyu Chen <sup>2</sup> and Fangzhi Huang <sup>2,\*</sup> <sup>1</sup> Department of Chemical and Chemical Engineering, Hefei Normal University, Hefei 230601, China<sup>2</sup> Lab of Clean Energy & Environmental Catalysis, Anhui Province Key Laboratory of Chemistry for Inorganic/Organic Hybrid Functionalized Materials, School of Chemistry and Chemical Engineering, Anhui University, Hefei 230601, China

\* Correspondence: huangfangzhi@163.com; Tel.: +86-551-63861328

**Abstract:** Removal rate and durability are the two most important parameters of an ideal air purification filter to remove inhalable particles and toxic gases. Here, based on the interaction of a local electric field and an external electric field, a novel coaxial core-shell CuO@NH<sub>2</sub>-MIL-53(Al) nanowire array was synthesized on a rigid copper net, which was used to remove PM<sub>2.5</sub> and SO<sub>2</sub> simultaneously. The removal rates of PM<sub>2.5</sub> by the filter with and without an external electric field can reach 98.72% and 44.41%, respectively, and the adsorption capacity of SO<sub>2</sub> can reach 4.87 mol/m<sup>2</sup>. After repeated filtration and cleaning for 10 cycles, the air pollution removal efficiency can be kept almost stable.



**Citation:** Li, J.; Sun, Q.; Ping, Z.; Gao, Y.; Chen, P.; Huang, F. Electric Field-Driven Air Purification Filter for High Efficiency Removal of PM<sub>2.5</sub> and SO<sub>2</sub>: Local Electric Field Induction and External Electric Field Enhancement. *Atmosphere* **2022**, *13*, 1260. <https://doi.org/10.3390/atmos13081260>

Academic Editors: Chang Wen, Youjian Zhu and Yishu Xu

Received: 6 July 2022

Accepted: 21 July 2022

Published: 9 August 2022

**Publisher's Note:** MDPI stays neutral with regard to jurisdictional claims in published maps and institutional affiliations.



**Copyright:** © 2022 by the authors. Licensee MDPI, Basel, Switzerland. This article is an open access article distributed under the terms and conditions of the Creative Commons Attribution (CC BY) license (<https://creativecommons.org/licenses/by/4.0/>).

**Keywords:** air purification filter; nanowire array; electric field; PM<sub>2.5</sub>; SO<sub>2</sub>

## 1. Introduction

Air pollution consisting of particles, droplets, gases or mixtures of the above substances has recently attracted serious attention due to its hazardous threat to public safety and health [1–4]. Among solid pollutants, fine particulate matter such as particulate matter 2.5 (PM<sub>2.5</sub>, diameter 2.5 μm or less) is the most harmful. SO<sub>x</sub> (i.e., SO<sub>2</sub>), one of the main gaseous pollutants, has a significant negative effect on human health and can lead to lung cancer [5–8]. What is more, SO<sub>2</sub> can also indirectly lead to the growth of PM<sub>2.5</sub> [9]. Various strategies have been developed to accomplish air purification, such as use of an electrostatic precipitator, bag dust collection and electro spun polymer [10–13]. Among them, electrostatic precipitation or adsorption has the advantages of low pressure drop and high collection efficiency, and has become one of the most promising technologies [14–19]. To improve the trapping efficiency, increasing the specific surface area of filter materials has gradually aroused great concern [20,21]. Therefore, most strategies adopt a honeycomb or porous structure, but this has the disadvantage of increased back pressure [22]. In recent research, in order to eliminate the disadvantage of traditional electrostatic adsorption filters, which cannot filter volatile organic compounds and toxic gases, a large number of activated carbon particles are fixed on the adsorption frame and embedded in the filtration system, thus realizing simultaneous adsorption of volatile organic compounds and toxic gases [23–26].

Metal–organic frameworks (MOFs) are types of mixed crystalline porous materials with large surface areas and adjustable pore diameter, which are beneficial to the capture of gaseous air pollutants, and the polar groups on their ligands are donated to give the filter the activity of adsorbing toxic gases [27–32]. For example, Wang et al. [33] processed MOF nanocrystals with porous structure into nanofiber filters with high porous MOF loadings, showing high particle removal efficiency and selectively capturing and retaining

SO<sub>2</sub>. However, the local electrostatic field of MOF is easily saturated or eliminated, and it is difficult to achieve long-term removal effects by local electrostatic precipitation or adsorption only. Based on the excellent electrical properties of metal nanowires, researchers have developed a polyvinylidene fluoride modified silver nanowire percolation network for filtration. In an electric field, these charged films strongly attract charged PM<sub>2.5</sub>, resulting in the effective removal performance of PM<sub>2.5</sub>. Compared with the particle filter based on short-range intermolecular force (local electrostatic field) used in the previous research, the particle filter based on long-range electrostatic interaction can not only remove PM<sub>2.5</sub> efficiently, but also can be reused [34].

Herein, we present an in-situ growth method to prepare a copper-mesh-supported coaxial core-shell CuO@NH<sub>2</sub>-MIL-53(Al) nanowire array. In this case, a large number of activated NH<sub>2</sub>-MIL-53 porous membranes are embedded into the filtration system through CuO nanowire arrays supported by copper mesh with excellent conductivity, thus realizing the combination of long-range electrostatic interaction and short-range electrostatic interaction and achieving excellent removal efficiency of PM<sub>2.5</sub> and SO<sub>2</sub>. Furthermore, it can be reused many times, thus making it a promising material for air quality control.

## 2. Materials and Methods

### 2.1. Materials

Aluminum chloride hexahydrate (AlCl<sub>3</sub>·6H<sub>2</sub>O, 97%, AR) and 2-Aminoterephthalic Acid (NH<sub>2</sub>-BDC, C<sub>8</sub>H<sub>7</sub>NO<sub>4</sub>) were all obtained from Aladdin Industrial Co. Ltd. (Shanghai, China). Poly(vinylpyrrolidone) (PVP) were purchased from Aladdin Industrial Co. Ltd. (Shanghai, China). Copper mesh (400 mesh) was obtained from Shanghai Yuren Co. Ltd. (Shanghai, China). Ultra-pure water with a resistivity of 18.2 MΩ cm used was provided by Millipore system.

### 2.2. Synthesis of Copper-Mesh-Supported CuO Nanowire Arrays

Highly ordered CuO nanowire arrays were synthesized via two-step method. First, vertical Cu(OH)<sub>2</sub> nanowire arrays were grown in situ on copper mesh according to our previous reports. Then, the obtained copper-mesh-supported Cu(OH)<sub>2</sub> nanowire arrays were calcined at 180 °C for 60 min, and further naturally cooled to room temperature. After this, copper-mesh-supported CuO<sub>2</sub> nanowire arrays were obtained.

### 2.3. Synthesis of Copper-Mesh-Supported CuO@NH<sub>2</sub>-MIL-53(Al) NWAs

The copper-mesh-supported CuO<sub>2</sub> NWAs were dipped into a 2 g/L of PVP solution for 30 min. After washed by water, it was immersed into 45.0 mL of 1mmol/L AlCl<sub>3</sub>·6H<sub>2</sub>O aqueous solution for 40 min to introduce Al<sup>3+</sup> ions on the surface of CuO nanowires. Then the pretreatment mesh was put into 45.0 mL of NH<sub>2</sub>-BDC N,N-Dimethylformamide (DMF) solution, and heated at 150 °C for 6 h under autogenous pressure. After cooling naturally, the as-prepared substrate was drawn from the reactions and washed with DMF and ethanol several times, respectively, and dried under vacuum at 30 °C.

### 2.4. PM<sub>2.5</sub> Filtration Test

The PM<sub>2.5</sub> filtration experiment was carried out as the following. The mixture of PM<sub>2.5</sub> and moisture was introduced into the left glass of the experiment setup. The inflow concentration was controlled by burning a cigarette to continuously induce a hazardous pollution level equivalent to the PM<sub>2.5</sub> index > 999 μg/m<sup>3</sup>. The PM<sub>2.5</sub> density was measured by a particle monitor (Xiaomi Technology Co., Ltd., China). Meanwhile, the pressure drop in the PM<sub>2.5</sub> filtration process was measured by a pressure drop detector (AC50, Smart Sensor, China) under a uniform airflow. The negative ionizer of 3V (XHJ-D05F) was placed for charging PM<sub>2.5</sub>. The PM<sub>2.5</sub> removal efficiency was calculated according to the following equation: where C<sub>0</sub> (ug.m<sup>3</sup><sup>-</sup>) and C<sub>1</sub> (ug.m<sup>3</sup><sup>-</sup>) are the PM<sub>2.5</sub> mass concentrations before and after PM<sub>2.5</sub> filtration, respectively. C<sub>0</sub> generated from incense per minute was a PM<sub>2.5</sub> simulated calculation value. By controlling the switching of the applied voltage and

negative ionizer, we can obtain the  $PM_{2.5}$  filtration efficiency of the  $CuO@NH_2-MIL-53(Al)$  filter at zero electric field and a certain electric field, respectively. The effective filtration test area of the  $CuO@NH_2-MIL-53(Al)$  filter was  $5.3\text{ cm}^2$ .

### 2.5. $SO_2$ Filtration Test

GC-MS (TSQ8000EVO) was performed to measure the absorption performance for  $SO_2$  of the  $CuO@NH_2-MIL-53(Al)$  filter. GC-MS sample bottle where one fourth filter with test area of  $3.06\text{ cm}^2$  was injected with 10 mL  $SO_2/N_2$  mixture (1%), and GC-MS was employed to measure the remaining  $SO_2$  concentration in the sample bottle after 5 min, 10 min, 20 min, 30 min, 40 min, 50 min, and 60 min, dynamically. Thus, the  $SO_2$  adsorption rate and capacity of the  $CuO@NH_2-MIL-53(Al)$  filter can be obtained by dynamically calculating the  $SO_2$  adsorption value.

### 2.6. Characterizations

The morphology was investigated by a Zeiss Supra 40 scanning electron microscope (SEM). The element distribution in nanowires was performed using energy-dispersive X-ray spectroscopy (EDS). Transmission electron microscope (TEM) was characterized with a JEOL JEM-2010-TEM. Thermogravimetric (TG) analysis was performed using a TG Q2000 analyzer from 25 to  $800\text{ }^\circ\text{C}$  under argon flow with a heating rate of  $10\text{ }^\circ\text{C min}^{-1}$ . The specific surface area and pore size were measured from ASAP2020M+C BET surface analyzer. The Fourier infrared spectra (FT-IR) ranging from  $500\text{ cm}^{-1}$  to  $4000\text{ cm}^{-1}$  were obtained with an infrared spectrometer (U-4100). The zeta potential was measured with Malvine nanometer laser particle size analyzer (Mastersizer 2000). The CA is the angle quantifying the wettability of a solid surface, which was performed on an OCA-20 contact angle analyzer (Data-Physics, Filderstadt, Germany).

## 3. Discussion

The coaxial  $CuO@NH_2-MIL-53(Al)$  nanowire arrays on porous copper mesh (NWAs/CM) was prepared by following a procedure involving in situ growth and self-assembly as illustrated in Figure 1a. Copper mesh was chosen as the supporting substrate on account of its excellent electrical conductivity, rigid property, and porous skeleton. Firstly, well-aligned  $Cu(OH)_2$  nanowires were directly grown on the skeleton of the copper mesh by a surface oxidation process (Figure S1, see Supporting Information). After a calcination treatment, the color of the samples turned to gray and the  $Cu(OH)_2$  completely converted to  $CuO$  (Figure 1b,c). The  $CuO$  nanowires with a diameter of 114 nm were vertically grown on the mesh substrate with a high cover density. As shown in Figure 1d, the water angle of the droplet on the  $CuO$  nanowire membrane was  $15.3^\circ$ , indicating a good hydrophilicity. After coating with the  $NH_2-MIL-53(Al)$  layer, the diameter of the nanowires increased to 159 nm, and the surface became rougher. Noticeably, the water angle of the droplet on this substrate was smaller than that of  $10^\circ$ , indicating the improvement of the surface hydrophilicity after the loading of the  $NH_2-MIL-53(Al)$  layer onto the  $CuO$  nanowires. Such a coaxial core-shell configuration can be confirmed by TEM images, as displayed in Figure 1h. It can be seen that the thickness of the discrete shell is about 43 nm. EDS mapping analysis as shown in Figure 1i-m further confirmed the coaxial core-shell structure. In comparison with Cu (yellow) located at the inner region, Al (purple), N (green) and O (blue) distributed uniformly in the whole nanowire area. The corresponding FT-IR spectra suggest the sharp bands at  $3380\text{ cm}^{-1}$  and  $3500\text{ cm}^{-1}$  are assigned the symmetric and asymmetric N-H vibrations, respectively, further indicating the  $NH_2-MIL-53(Al)$  loading (Figure S2). The mass loading of  $NH_2-MIL-53(Al)$  in the composite nanowires was calculated ca. 10.13 wt.% from the TG analysis (Figure S3). The results suggest well-defined coaxial  $CuO@NH_2-MIL-53(Al)$  NWAs/CM have been successfully grown on the copper mesh by the integrated method.

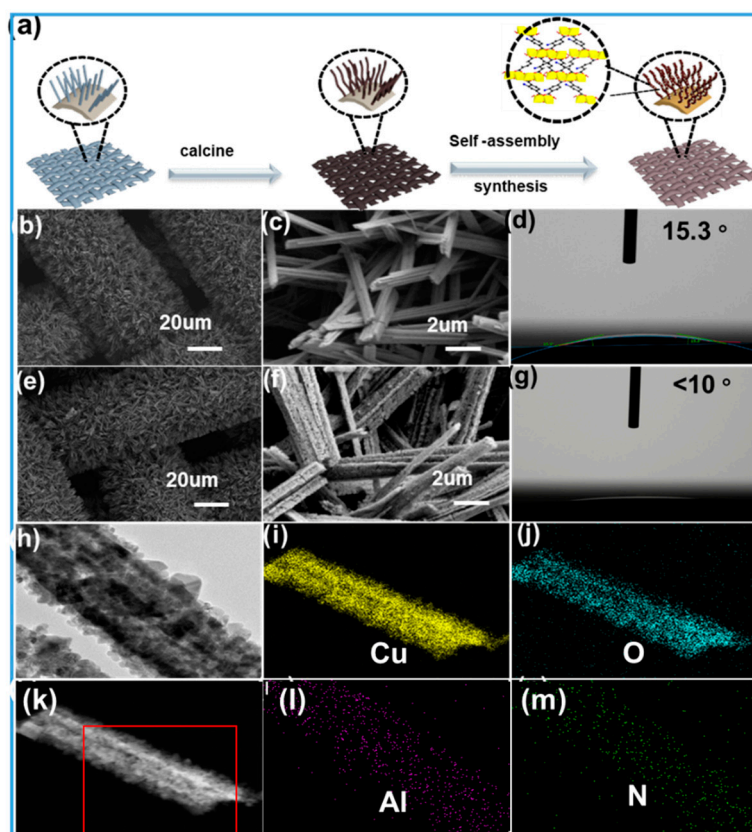


**Figure 1.** (a) Schematic illustration of the formation process of core-shell CuO@NH<sub>2</sub>-MIL-53(Al) nanowires grown on 400 copper mesh. (b,c) Different magnification SEM images of CuO nanowires and (e,f) core-shell CuO@NH<sub>2</sub>-MIL-53(Al) nanowires grown on 400 copper mesh. (d,g) The respective water contact angles of CuO and CuO@NH<sub>2</sub>-MIL-53(Al) nanowire arrays. (h) High-resolution TEM graph of a single core-shell CuO@NH<sub>2</sub>-MIL-53 nanowire. (k) TEM graph of a single core-shell CuO@NH<sub>2</sub>-MIL-53 nanowire, and the red frame is the actual sampling range of EDS. (i–m) Elemental mapping images of Cu, O, Al, and N record from the same zone.

The interfacial properties of the coaxial core-shell CuO@NH<sub>2</sub>-MIL-53(Al) NWAs/CM will directly affect its adsorption performance for air pollutants. Firstly, the BET surface areas and porous structures of the CuO NWAs/CM and CuO@NH<sub>2</sub>-MIL-53(Al) NWAs/CM were determined by N<sub>2</sub> adsorption/desorption isotherms. As shown in Figure S4, it is clearly seen that the N<sub>2</sub> adsorption/desorption isotherms of CuO NWAs/CM is a typical nonporous adsorption curve of type II, but there is a typical Hysteresis (H3) loop, which indicates that capillary condensation may exist in the array structure. After the NH<sub>2</sub>-MIL-53(Al) is wrapped onto the CuO nanowires, there is a typical IV adsorption isotherm with H1 ring, indicating that mesoporous adsorption and capillary adsorption coexist. The surface charge of the CuO@NH<sub>2</sub>-MIL-53(Al) NWAs/CM was evaluated by  $\zeta$  potential detection. The  $\zeta$  potential of CuO@NH<sub>2</sub>-MIL-53(Al) NWAs/CM was measured at about +23.6 mV in aqueous solution, indicating an interface with electronegativity. In summary, we have constructed a positively charged superhydrophilic interface on the surface of copper mesh with certain adsorption properties. Furthermore, the electrical properties of the copper mesh interface are mainly derived from amino groups and have a strong interaction with acidic toxic gases such as sulfur dioxide. Thus, the air filter system is designed to collect PM<sub>2.5</sub> and SO<sub>2</sub> in a more active manner by electrostatic force when a voltage is applied to the CuO@NH<sub>2</sub>-MIL-53(Al) NWAs/CM filter. Compared with the short-range intermolecular force used in the previous research on polarized polymer nanofiber particle filters, when low electric energy is applied, the CuO@NH<sub>2</sub>-MIL-53(Al) NWAs/CM filter uses long-range electrostatic force and short-range electrostatic force, which can not

only collect particulate matter more effectively, but also complete the efficient collection of toxic gases at the same time.

The schematic diagram and test device for measuring the PM<sub>2.5</sub> capture efficiency were displayed in Figure 2a,b, respectively. Specifically, as shown in Figure 2a, the whole device consists of an air inlet, a modified copper net, an air outlet and a detection system in turn. Firstly, a filter was fixed at the joint of two glasses. The thickness of one layer of the filter is 64 μm (Figure 2c), and the rigid-thin-layer ensures that fresh air can easily pass through. Subsequently, a PM<sub>2.5</sub> detector was placed in the right glass of the experimental device to measure the concentration of PM<sub>2.5</sub>, and a 1.5 V negative ion generator was placed in the left glass of the experimental device to negatively charge PM<sub>2.5</sub>. Finally, the left fan acts as a suction force from left to right, and the pressure drop is measured by a pressure gauge. When the voltage applied to the filter is positively charged, an electric field will be established between the filter and PM<sub>2.5</sub>. The performance of the filter in removing PM<sub>2.5</sub> was tested under and without an external electric field, respectively. As shown in Figure 2e, the PM<sub>2.5</sub> removal efficiency of the Cu mesh filter, CuO NWAs/CM filter and CuO@NH<sub>2</sub>-MIL-53(Al) NWAs/CM filter was 1.7%, 12.25%, and 44.41%, respectively, indicating that the uniform growth of CuO nanowire arrays and NH<sub>2</sub>-MIL-53(Al) on the CuO nanowire arrays all can significantly improve the filtration efficiency. The different mass changes with 0~60 min adsorption time that occurred in the CuO@NH<sub>2</sub>-MIL-53(Al) filter under zero field and a certain electric field were compared in Figure 2c. The mass changes with 0~60 min adsorption time that occurred in the pure Cu mesh, CuO membrane and CuO@NH<sub>2</sub>-MIL-53(Al) membrane under zero field and a certain electric field were further compared in Figure S5. The digital images and SEM images of the as-prepared CuO@NH<sub>2</sub>-MIL-53(Al) filter before and after the 60 min PM<sub>2.5</sub> capture test under the electric field were, respectively, exhibited in Figure 2f, indicating an excellent PM<sub>2.5</sub> removal performance in our air filter under the influence of the electric field. The corresponding SEM image (Figure S6) of the CuO@NH<sub>2</sub>-MIL-53(Al) NWAs/CM filter after capturing PM<sub>2.5</sub> shows that more and more PM<sub>2.5</sub> is captured with the increase in adsorption time. Interestingly, during the adsorption process, PM<sub>2.5</sub> was uniformly adsorbed on the surface of nanowires without tip effect. While, after applied a certain electric field, the removal efficiency of the Cu mesh, CuO membrane and CuO@NH<sub>2</sub>-MIL-53(Al) filter was greatly improved to 73.39%, 86.17% and 98.72%, respectively, indicating strong PM filtration capability. Compared with the highest-level medical protective mask material of melt-blown cloth (>95%) or polymer nanofiber network particle filter (95–99%), the CuO@NH<sub>2</sub>-MIL-53(Al) filter shows a high efficiency (>98.72%) [14].

Furthermore, as shown in Figure 3, SEM image of the CuO@NH<sub>2</sub>-MIL-53(Al) NWAs/CM filter after capturing PM<sub>2.5</sub> shows that the most important contribution during the adsorption process is tip adsorption. Due to tip adsorption, spherical-like aggregates with particle sizes of 1–2 microns can be formed on the top of the nanowires, which can not only intercept a large amount of PM<sub>2.5</sub> but also cannot block the gaps in the CuO@NH<sub>2</sub>-MIL-53(Al) NWAs/CM filter. Therefore, even if a large amount of PM<sub>2.5</sub> is trapped, the filter still has good air permeability. What is more, even after 10 cycles of ethylene glycol washing, the removal efficiency has virtually no obvious change and still reaches 97.46% (Figure 2g). PM<sub>2.5</sub> aggregates are easily cleaned due to the good solubility of PM<sub>2.5</sub> in highly polar solvents (Figure 3f), and the CuO@NH<sub>2</sub>-MIL-53(Al) filter will not be damaged even after repeated cleaning, which ensures the reusability of the CuO@NH<sub>2</sub>-MIL-53(Al) filter. However, with repeated use after continuous washing, the removal efficiency of the CuO@NH<sub>2</sub>-MIL-53(Al) NWAs/CM filter tends to decrease under the action of no electric field, and drops to 38.65% after 10 repetitions (Figure 2f). All this may be due to the mechanism in Figure 4. As shown in Figure 4, the filtering membrane mainly filters PM<sub>2.5</sub> through interception, inertial collision, Brownian diffusion and gravity sedimentation without applying an electric field. Moreover, during the filtration process, due to the hydrophilicity of the filter surface and the fact that NH<sub>2</sub><sup>−</sup> groups easily form positively charged NH<sub>3</sub><sup>+</sup> (the ζ potential is +23.6 mV), the filter surface is easy capable of generating relatively weak intermolecular forces such

as short-range electrostatic force or van der Waals force with the permanent dipoles of  $PM_{2.5}$  to capture  $PM_{2.5}$ . However, it is well known that with repeated use, the short-range electrostatic force will gradually decrease and cause the  $PM$  removal rate to decrease [14,15]. When a positive voltage is applied to the core-shell  $CuO@NH_2-MIL-53(Al)$  nanowires of the filter to permeate the network. At the same time,  $PM_{2.5}$  is generated from the incense and negatively charged by the ionizer. Thus, an electric field is built between the filter and  $PM_{2.5}$ , and a strong long-range electrostatic attraction is generated between the  $CuO@NH_2-MIL-53(Al)$  NWAs/CM filter and  $PM_{2.5}$  was described in the following Equation and Figure 3b.

$$F_e = K_e (q_1 q_2 / r + Q_1 Q_2 / R)$$

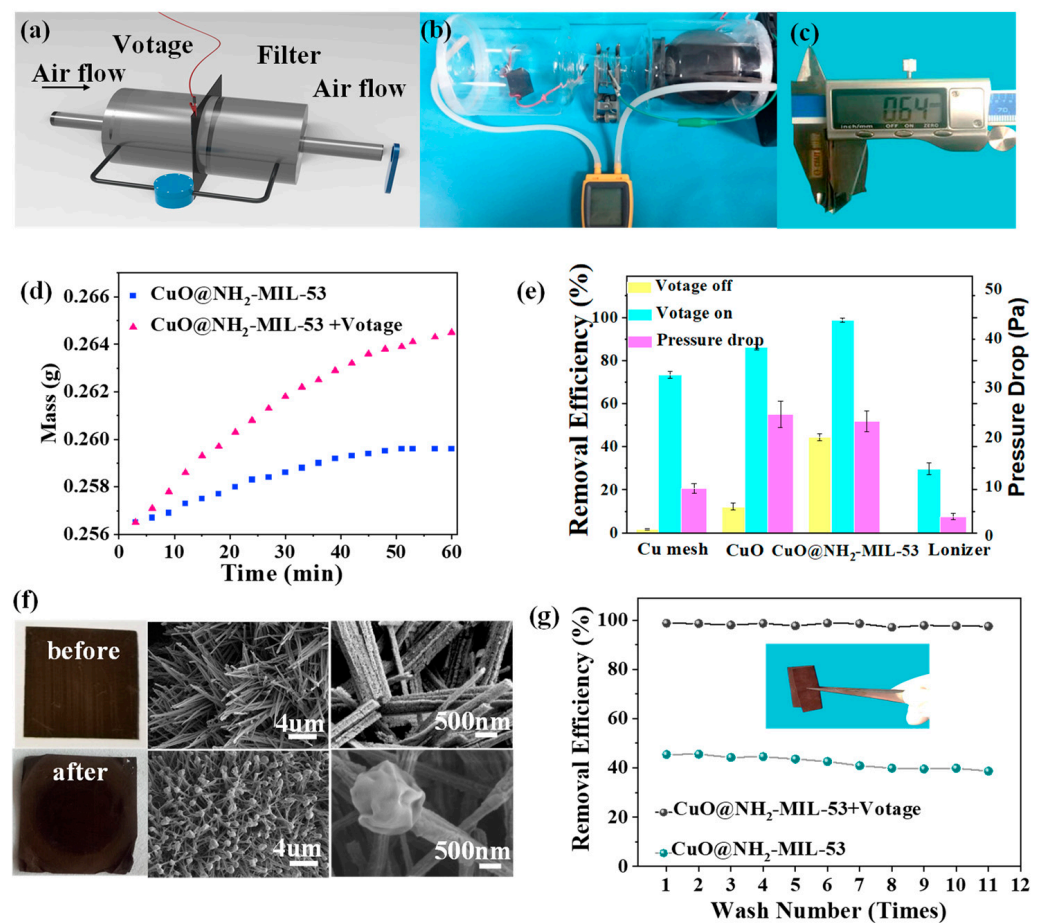


**Figure 2.** (a) Schematic diagram and (b) test device. (c) photo-image of the experimental setup for measuring the  $PM_{2.5}$  removal filter. (d)  $PM_{2.5}$  filtration efficiency of the pure Cu mesh, CuO and  $CuO@NH_2-MIL-53(Al)$  membranes at an applied electric field and zero electric field. (e) The areal mass change of the  $CuO@NH_2-MIL-53(Al)$  filter after  $PM_{2.5}$  capture with different adsorption time at an applied electric field and zero electric field. (f) Photos and SEM images of the  $CuO@NH_2-MIL-53(Al)$  filter before and after  $PM_{2.5}$  capture at an applied electric field. (g) Repeated  $PM_{2.5}$  removal performance test of  $CuO@NH_2-MIL-53(Al)$  membrane at zero electric field and applied electric field.

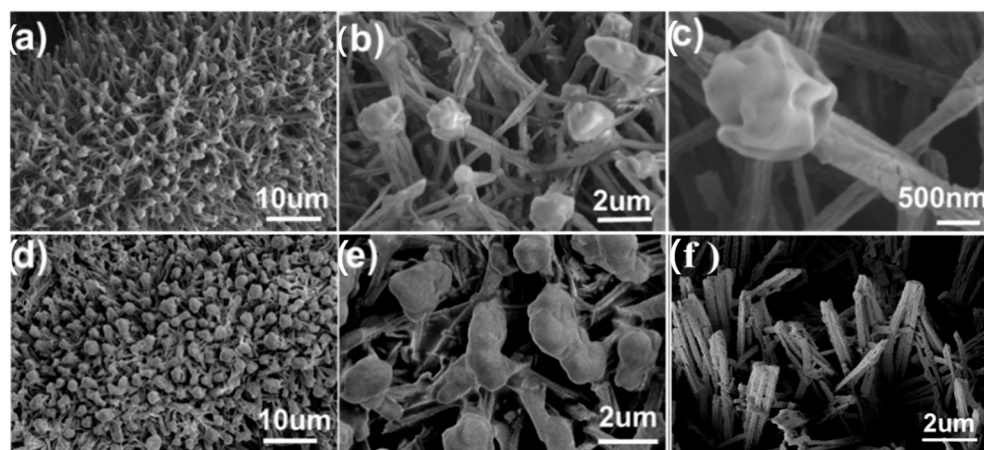


**Figure 3.** SEM images of the CuO@NH<sub>2</sub>-MIL-53(Al) filter with different time of PM<sub>2.5</sub> capture under an applied electric field. (a–c) 30 min, (d,e) 60 min, and (f) after ethylene glycol washing.

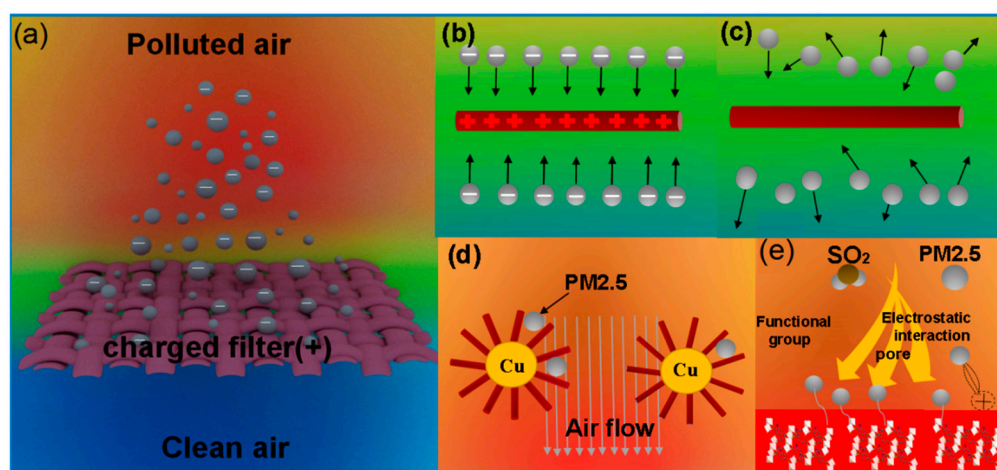


**Figure 4.** Illustration of the PM<sub>2.5</sub> capture process. (a) Schematic of the CuO@NH<sub>2</sub>-MIL-53(Al) filter capturing PM<sub>2.5</sub>. (b) Schematic of electrostatic precipitation which captures PM<sub>2.5</sub> of the CuO@NH<sub>2</sub>-MIL-53(Al) nanowires at an applied electric field. (c) CuO@NH<sub>2</sub>-MIL-53(Al) nanowires at zero electric field. (d) Filtration schematic of CuO@NH<sub>2</sub>-MIL-53(Al) nanowires of the PM<sub>2.5</sub> capture mechanism filtrating PM<sub>2.5</sub>. (e) Proposed capture mechanism of the filter for PM<sub>2.5</sub> and SO<sub>2</sub>.

$K_e$  is Coulomb's constant,  $q_1$  and  $q_2$  are the magnitudes of the charges which can generate short-range electrostatic interaction,  $Q_1$  and  $Q_2$  are the magnitudes of the charges which can generate long-range electrostatic interaction, and  $r$ ,  $R$  are the distances between two charges with different properties, respectively. Therefore, under the action of an applied electric field, the removal process of PM<sub>2.5</sub> depends on the synergistic effect of long-range electrostatic interaction and short-range electrostatic interaction between the CuO@NH<sub>2</sub>-MIL-53(Al) NWAs/CM filter and PM<sub>2.5</sub>, resulting in more particles being adsorbed on the net and intercepted instead of being merely blocked. The remote electrostatic interaction force generated by the applied electric field plays a leading role in the filtration system and is both controllable and unaffected by the interface properties of materials. Therefore, under the condition of an external electric field, the filtering membrane can be reused without lowering the removal rate.

In addition to PM<sub>2.5</sub> capture, the CuO@NH<sub>2</sub>-MIL-53 (aluminum) filter is also designed to adsorb SO<sub>2</sub>, which is one of the most dangerous and common gaseous pollutants. The SO<sub>2</sub> adsorption performance of the CuO@NH<sub>2</sub>-MIL-53 filter and the adsorption capacity per unit area of the filter were measured by gas chromatography-mass spectrometry, as shown in Figure 5a. The adsorption curve shows that the filter has a high adsorption

speed in the first 20 min and reaches an adsorption saturation of  $4.87 \text{ mol/m}^2$  after about 60 min, which fully conforms to the Langmuir formula. Furthermore, Figure 5b indicates the filter can be reused and retained a stable  $\text{SO}_2$  adsorption performance of  $3.6 \text{ mol/m}^2$  after three cycles of the adsorption–desorption procedure by regenerating the filter under  $\text{N}_2$  flow for 12 h at  $25^\circ\text{C}$ . The excellent adsorption capacity of the  $\text{CuO@NH}_2\text{-MIL-53(Al)}$  prepared in our work is owing to the enhanced porosity, smaller pore size of  $\text{CuO@NH}_2\text{-MIL-53(Al)}$  (Figure S4a). Additionally, the dynamic diameter of  $\text{SO}_2$  is  $3.6 \text{ \AA}$ , while the pore size of the  $\text{CuO@NH}_2\text{-MIL-53(Al)}$  prepared in our work is  $18 \text{ \AA}$  (Figure S4b). Besides, the amine radicals of  $\text{CuO@NH}_2\text{-MIL-53(Al)}$  played a crucial role in acidic polar gas species adsorption. As shown in Figure S7, the  $\text{CuO@NH}_2\text{-MIL-53(Al)}$  filter exhibited a superior  $\text{SO}_2$  adsorption performance to the  $\text{CuO@MIL-53(Al)}$  filter, suggesting that the amino-groups in  $\text{CuO@NH}_2\text{-MIL-53(Al)}$  improved the performance in acidic polar gases adsorption due to every MIL-53(Al) unit cooperating with amino-groups.

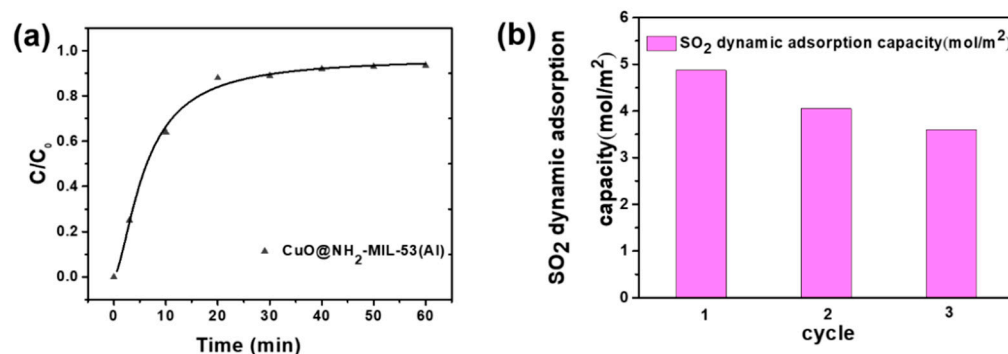


**Figure 5.** (a)  $\text{SO}_2$  adsorption performance of  $\text{CuO@NH}_2\text{-MIL-53(Al)}$  filter. (b) Cycle performance of the  $\text{CuO@NH}_2\text{-MIL-53(Al)}$  filter after regenerating under a  $\text{N}_2$  flow at  $25^\circ\text{C}$ .

#### 4. Conclusions

In this work, we presented a copper-mesh-supported coaxial core–shell  $\text{CuO@NH}_2\text{-MIL-53(Al)}$  nanowire array filter combining excellent  $\text{PM}_{2.5}$  and  $\text{SO}_2$  removal abilities simultaneously. The removal rates of  $\text{PM}_{2.5}$  by the coaxial core–shell  $\text{CuO@NH}_2\text{-MIL-53(Al)}$  NWAs/CM filter with and without an external electric field are 98.72% and 44.41%, respectively. In addition, the filter can adsorb  $\text{SO}_2$  selectively and effectively when exposed in 1%  $\text{SO}_2/\text{N}_2$  mixture, demonstrating an excellent capacity of  $4.87 \text{ mol/m}^2$ . The  $\text{CuO@NH}_2\text{-MIL-53(Al)}$  filter was found to still retain a dynamic efficiency for air pollution even after cycling several times, indicating that it can be potentially applied to the effective improvement of air clean.

**Supplementary Materials:** The following supporting information can be downloaded at: <https://www.mdpi.com/article/10.3390/atmos13081260/s1>.

**Author Contributions:** J.L.: Conceptualization, Investigation, Formal analysis, Data curation, Methodology, Writing—review & editing. Q.S.: Conceptualization, Investigation, Formal analysis, Data curation, Validation, Writing—original draft. Z.P.: Formal analysis, Data curation. Y.G.: Formal analysis. P.C.: Investigation. F.H.: Conceptualization, Data curation, Formal analysis, project administration, Funding acquisition, Resources, Supervision. All authors have read and agreed to the published version of the manuscript.

**Funding:** This work was supported by the National Natural Science Foundation of China (21771001), Key projects of quality engineering teaching and research in Anhui Province (2018jyxm0365), the Program of Anhui Scientific and Technical Leaders Reserve Candidates (2018H168), the Scholar Program for the Outstanding Innovative Talent of College Discipline (Specialty), and open fund for Discipline Construction, Institute of Physical Science and Information Technology, Anhui University.

**Institutional Review Board Statement:** Not applicable.

**Informed Consent Statement:** Not applicable.

**Data Availability Statement:** Not applicable.

**Conflicts of Interest:** The authors declare no conflict of interest.

## References

1. Rahman, M.; Thurston, G. A hybrid satellite and land use regression model of source-specific PM<sub>2.5</sub> and PM<sub>2.5</sub> constituents. *Environ. Int.* **2022**, *163*, 107233. [[CrossRef](#)] [[PubMed](#)]
2. Xue, T.; Liu, J.; Zhang, Q.; Geng, G.; Zheng, Y.; Tong, D.; Liu, Z.; Guan, D.; Bo, Y.; Zhu, T.; et al. Rapid Improvement of PM<sub>2.5</sub> Pollution and Associated Health Benefits in China During 2013–2017. *Sci. China Earth Sci.* **2019**, *62*, 1847–1856. [[CrossRef](#)]
3. Azevedo, R.S.S.; de Sousa, J.R.; Araujo, M.T.F.; Martins Filho, A.J.; de Alcantara, B.N.; Araujo, F.M.C.; Queiroz, M.G.L.; Cruz, A.C.R.; Vasconcelos, B.H.B.; Chiang, J.O.; et al. In situ immune response and mechanisms of cell damage in central nervous system of fatal cases microcephaly by zika virus. *Sci. Rep.* **2018**, *8*, 1–11. [[CrossRef](#)] [[PubMed](#)]
4. Wang, G.C.; Shi, Q.; Wang, H.; Sun, K.Z.; Lu, Y.X.; Di, K.X. Multi-modal image feature fusion-based PM<sub>2.5</sub> concentration estimation. *Atmos. Pollut. Res.* **2022**, *13*, 101345. [[CrossRef](#)]
5. Kampa, M.; Castanas, E. human health effects of air pollution. *Environ. Pollut.* **2008**, *151*, 362–367. [[CrossRef](#)]
6. Evans, J.; van Donkelaar, A.; Martin, R.V.; Burnett, R.; Rainham, D.G.; Birkett, N.J.; Krewski, D. Estimates of global mortality attributable to particulate air pollution using satellite imagery. *Environ. Res.* **2013**, *120*, 33–42. [[CrossRef](#)] [[PubMed](#)]
7. Gaffney, J.S.; Streit, G.E.; Spall, W.D.; Hall, J.H. Beyond Acid Rain. Do Soluble Oxidants and Organic Toxins interact with SO<sub>2</sub> and NO<sub>x</sub> to Increase Ecosystem Effects? *Environ. Sci. Technol.* **1987**, *21*, 519–524. [[CrossRef](#)]
8. Turner, M.C.; Krewski, D.; Pope, C.A., 3rd; Chen, Y.; Gapstur, S.M.; Thun, M.J. Long-Term Ambient Fine Particulate Matter Air Pollution and Lung Cancer in a Large Cohort of Never-Smokers. *Am. J. Respir. Crit Care Med.* **2011**, *184*, 1374–1381. [[CrossRef](#)] [[PubMed](#)]
9. Zhang, L.; Jin, X.; Johnson, A.C.; Giesy, J.P. Hazard Posed by Metals and As in PM<sub>2.5</sub> in Air of Five Megacities in the Beijing-Tianjin-Hebei Region of China During APEC. *Environ. Sci. Pollut. Res. Int.* **2016**, *23*, 17603–17612. [[CrossRef](#)]
10. Xiao, J.; Liang, J.; Zhang, C.; Tao, Y.; Ling, G.-W.; Yang, Q.-H. Advanced Materials for Capturing Particulate Matter: Progress and Perspectives. *Small Methods* **2018**, *2*, 1800012. [[CrossRef](#)]
11. Trakumas, S.; Willeke, K.; Reponen, T.; Grinshpun, S.A.; Friedman, W. Comparison of Filter Bag, Cyclonic, and Wet Dust Collection Methods in Vacuum Cleaners. *AIHAJ-Am. Ind. Hyg. Assoc.* **2001**, *62*, 573–583. [[CrossRef](#)]
12. Grass, N.; Hartmann, W.; Klockner, M. Application of Different Types of High-Voltage Supplies on Industrial Electrostatic Precipitators. *IEEE Trans. Ind. Appl.* **2004**, *40*, 1513–1520. [[CrossRef](#)]
13. Park, J.-S. Electrospinning and its applications. *Adv. Nat. Sci. Nanosci. Nanotechnol.* **2011**, *1*, 043002. [[CrossRef](#)]
14. Liu, J.; Ren, B.; Wang, Y.; Lu, Y.; Wang, L.; Chen, Y.; Yang, J.; Huang, Y. Hierarchical Porous Ceramics with 3D Reticular Architecture and Efficient Flow-Through Filtration Towards High-Temperature Particulate Matter Capture. *Chem. Eng. J.* **2019**, *362*, 504–512. [[CrossRef](#)]
15. Bai, Y.; Han, C.B.; He, C.; Gu, G.Q.; Nie, J.H.; Shao, J.J.; Xiao, T.X.; Deng, C.R.; Wang, Z.L. Washable Multilayer Triboelectric Air Filter for Efficient Particulate Matter PM<sub>2.5</sub> Removal. *Adv. Funct. Mater.* **2018**, *28*, 1706680. [[CrossRef](#)]
16. Khalid, B.; Bai, X.; Wei, H.; Huang, Y.; Wu, H.; Cui, Y. Direct Blow-Spinning of Nanofibers on a Window Screen for Highly Efficient PM<sub>2.5</sub> Removal. *Nano Lett.* **2017**, *17*, 1140–1148. [[CrossRef](#)]
17. Jeong, S.; Cho, H.; Han, S.; Won, P.; Lee, H.; Hong, S.; Yeo, J.; Kwon, J.; Ko, S.H. High Efficiency, Transparent, Reusable, and Active PM<sub>2.5</sub> Filters by Hierarchical Ag Nanowire Percolation Network. *Nano Lett.* **2017**, *17*, 4339–4346. [[CrossRef](#)]
18. Huang, W.R.; He, Z.; Wang, J.L.; Liu, J.W.; Yu, S.H. Mass Production of Nanowire-Nylon Flexible Transparent Smart Windows for PM<sub>2.5</sub> Capture. *iScience* **2019**, *12*, 333–341. [[CrossRef](#)]
19. Guo, W.; Zhang, X.; Yu, X.; Wang, S.; Qiu, J.; Tang, W.; Li, L.; Liu, H.; Wang, Z.L. Self-Powered Electrical Stimulation for Enhancing Neural Differentiation of Mesenchymal Stem Cells on Graphene-Poly(3,4-ethylenedioxythiophene) Hybrid Microfibers. *ACS Nano* **2016**, *10*, 5086–5095. [[CrossRef](#)]
20. Zhang, P.; Wan, D.; Zhang, Z.; Wang, G.; Hu, J.; Shao, G. RGO-Functionalized Polymer Nanofibrous Membrane with Exceptional Surface Activity and Ultra-Low Airflow Resistance for PM<sub>2.5</sub> Filtration. *Environ. Sci. Nano* **2018**, *5*, 1813–1820. [[CrossRef](#)]
21. Glover, T.G.; Peterson, G.W.; Schindler, B.J.; Britt, D.; Yaghi, O. MOF-74 Building Unit has a Direct Impact on Toxic Gas Adsorption. *Chem. Eng. Sci.* **2011**, *66*, 163–170. [[CrossRef](#)]
22. Xu, J.; Liu, C.; Hsu, P.C.; Liu, K.; Zhang, R.; Liu, Y.; Cui, Y. Roll-to-Roll Transfer of Electrospun Nanofiber Film for High-Efficiency Transparent Air Filter. *Nano Lett.* **2016**, *16*, 1270–1275. [[CrossRef](#)] [[PubMed](#)]
23. Liu, H.; Cao, C.; Huang, J.; Chen, Z.; Chen, G.; Lai, Y. Progress on Particulate Matter Filtration Technology: Basic Concepts, Advanced Materials, and Performances. *Nanoscale* **2020**, *12*, 437–453. [[CrossRef](#)] [[PubMed](#)]
24. Gu, G.Q.; Han, C.B.; Lu, C.X.; He, C.; Jiang, T.; Gao, Z.L.; Li, C.J.; Wang, Z.L. Triboelectric Nanogenerator Enhanced Nanofiber Air Filters for Efficient Particulate Matter Removal. *ACS Nano* **2017**, *11*, 6211–6217. [[CrossRef](#)] [[PubMed](#)]
25. Ma, X.; Chai, Y.; Li, P.; Wang, B. Metal-Organic Framework Films and Their Potential Applications in Environmental Pollution Control. *Accounts Chem. Res.* **2019**, *52*, 1461–1470.
26. Ma, S.; Zhang, M.; Nie, J.; Tan, J.; Yang, B.; Song, S. Design of Double-Component Metal-Organic Framework Air Filters with PM<sub>2.5</sub> Capture, Gas Adsorption and Antibacterial Capacities. *Carbohydr. Polym.* **2019**, *203*, 415–422. [[CrossRef](#)] [[PubMed](#)]

27. Feng, S.; Li, X.; Zhao, S.; Hu, Y.; Zhong, Z.; Xing, W.; Wang, H. Multifunctional Metal Organic Framework and Carbon Nanotube-Modified Filter for Combined Ultrafine Dust Capture and SO<sub>2</sub> Dynamic Adsorption. *Environ. Sci. Nano* **2018**, *5*, 3023–3031. [[CrossRef](#)]
28. Peterson, G.W.; Mahle, J.J.; DeCoste, J.B.; Gordon, W.O.; Rossin, J.A. Extraordinary NO<sub>2</sub> Removal by the Metal-Organic Framework UiO-66-NH<sub>2</sub>. *Angew. Chem.* **2016**, *55*, 6235–6238. [[CrossRef](#)]
29. Peterson, G.W.; DeCoste, J.B.; Fatollahi-Fard, F.; Britt, D.K. Engineering UiO-66-NH<sub>2</sub> for Toxic Gas Removal. *Ind. Eng. Chem. Res.* **2014**, *53*, 701–707. [[CrossRef](#)]
30. Zhao, J.; Nunn, W.T.; Lemaire, P.C.; Lin, Y.; Dickey, M.D.; Oldham, C.J.; Walls, H.J.; Peterson, G.W.; Losego, M.D.; Parsons, G.N. Facile Conversion of Hydroxy Double Salts to Metal-Organic Frameworks Using Metal Oxide Particles and Atomic Layer Deposition Thin-Film Templates. *J. Am. Chem. Soc.* **2015**, *137*, 13756–13759. [[CrossRef](#)] [[PubMed](#)]
31. Wisser, D.; Wisser, F.M.; Raschke, S.; Klein, N.; Leistner, M.; Grothe, J.; Brunner, E.; Kaskel, S. Biological Chitin-MOF Composites with Hierarchical Pore Systems for Air-Filtration Application. *Angew. Chem. Int. Ed.* **2015**, *54*, 12588–12591. [[CrossRef](#)] [[PubMed](#)]
32. Furukawa, H.; Cordova, K.E.; O’Keeffe, M.; Yaghi, O.M. The Chemistry and Applications of Metal-Organic Frameworks. *Science* **2013**, *341*, 1230444. [[CrossRef](#)] [[PubMed](#)]
33. Zhang, Y.; Yuan, S.; Feng, X.; Li, H.; Zhou, J.; Wang, B. Preparation of Nanofibrous Metal-Organic Framework Filters for Efficient Air Pollution Control. *J. Am. Chem. Soc.* **2016**, *138*, 5785–5788. [[CrossRef](#)] [[PubMed](#)]
34. Zhao, X.; Li, Y.; Hua, T.; Jiang, P.; Yin, X.; Yu, J.; Ding, B. Low-Resistance Dual-Purpose Air Filter Releasing Negative Ions and Effectively Capturing PM<sub>2.5</sub>. *ACS Appl. Mater. Interfaces* **2017**, *9*, 12054–12063. [[CrossRef](#)] [[PubMed](#)]